Scattering of 10–30 Mev Negative Pions by Hydrogen*

D. E. NAGLE,† R. H. HILDEBRAND, AND R. J. PLANO‡
The Enrico Fermi Institute for Nuclear Studies and Department of Physics, The University of Chicago, Chicago, Illinois
(Received October 15, 1956)

Fifty-seven π^--p scattering events in the energy range 10–30 Mev have been observed in a hydrogen bubble chamber. The S-wave scattering length $\frac{1}{3}\eta^{-1}(2\alpha_1+\alpha_3)=0.077\pm0.011$ is found to give the best fit to the data assuming $\alpha_{13}=\alpha_{31}=\alpha_{11}=0$, $\alpha_{33}=0.235\eta^3$. This result is combined with the results of other low-energy scattering experiments to give estimates of α_1 and α_3.

I. INTRODUCTION

THE elastic scattering of low-energy negative pions by protons has been studied in emulsions[1] and in a hydrogen-filled diffusion cloud chamber.[2] In this paper we report a hydrogen bubble-chamber measurement of the same process[3] which confirms the previous results and provides somewhat improved statistical accuracy. These experiments cover the energy range 2 to 30 Mev where S-wave scattering is dominant and where counter experiments are difficult because of the short range of the scattered particles.

From the scattering distributions one may obtain a value for the scattering length a_- which is related to the S-wave phase shifts by the expression $a_-=\frac{1}{3}\eta^{-1}(2\alpha_1+\alpha_3)$, where η is the pion momentum in units of $m_\pi c$ and α_1 and α_3 are the S-wave phase shifts for isotopic spins $\frac{1}{2}$ and $\frac{3}{2}$, respectively. Combining this result with recent low-energy positive pion scattering results, one may obtain values for α_1 and α_3 independently.

The assumptions and errors involved in the various low-energy nonexchange scattering experiments are sufficiently similar so that the results may be combined in a consistent way for any assumed P waves provided the original data are at hand. Accordingly, we shall present a complete list of our scattering events and other essential data in addition to our own analysis.

A review of the whole field of S-wave meson-nucleon interactions would have to discuss quite different types of assumptions and errors for other S-wave processes. Thus the charge-exchange experiments which have been performed involve either corrections for radiative capture[4] or counter geometry[5]; the photomeson production experiments[6] involve corrections for the effects of binding a neutron in a deuteron; and the pi-mesonic x-ray analysis[7] involves the assumption of additivity of the effects of the individual nucleons.

We make no attempt to examine the consistency of all the observations in this vast field. We confine this paper to remarks on the bubble-chamber technique, a presentation of the essential data of this measurement, and a brief summary of closely related experimental results.

II. HYDROGEN BUBBLE CHAMBER

A general account of the construction and operation of the bubble chamber has been given in a previous paper.[8] The features we shall emphasize here are those associated with the optical system and the bubble tracks.

The chamber itself has inside dimensions $2.5\times2.5\times10$ cm with the long axis parallel to the beam. A grid of lines is etched on the outer surfaces to provide a reference system for the tracks. These lines allow a measurement of the magnification of the optical system and are also used in focusing and aligning the cameras.

The cameras are arranged as shown in Fig. 1. When they are placed so that the grid lines in the centers of the near and far walls of the chamber appear superimposed, their optic axes are at $90°\pm0°15'$ to each other and to the beam. The accuracy of the alignment is determined

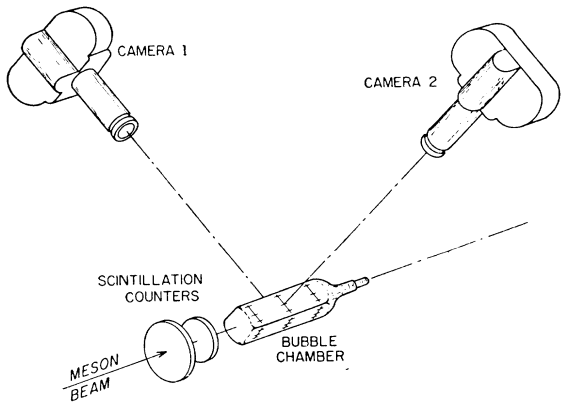

FIG. 1. Arrangement of counters, cameras, and bubble chamber.

* Research supported by a joint program of the Office of Naval Research and the U. S. Atomic Energy Commission.
† Now at Los Alamos Scientific Laboratory, Los Alamos, New Mexico.
‡ Now at Columbia University, New York, New York.
[1] Orear, Slater, Lord, Eilenberg, and Weaver, Phys. Rev. **96**, 174 (1954).
[2] Rinehart, Rogers, and Lederman, Phys. Rev. **100**, 883 (1955).
[3] A brief account of this experiment is contained in the *Proceedings of the CERN Symposium on High-Energy Accelerators and Pion Physics, June 1956* (to be published).
[4] W. Spry, Phys. Rev. **95**, 1295 (1954).
[5] J. Tinlot and A. Roberts, Phys. Rev. **95**, 137 (1954).
[6] G. Bernardini, *Proceedings of the CERN Symposium on High Energy Accelerators and Pion Physics, June 1956* (to be published).
[7] Stearns, Stearns, Di Benedetti, and Leipuner, Phys. Rev. **96**, 804 (1954); Camac, McGuire, Platt, and Schulte, Phys. Rev. **99**, 897 (1955).
[8] Nagle, Hildebrand, and Plano, Rev. Sci. Instr. **27**, 203 (1956).

by the optical resolution at the outside surfaces (about 10 lines/mm) and by the distance between the surfaces (3.4 cm).

The two pictures of the chamber can, in most cases, be treated as orthographic projections at 90° to each other so that the geometrical analysis is trivial. This is possible because the distance from the chamber to the camera lenses (110 cm) is very large compared to the dimensions of the chamber. In some cases small corrections must be made for point projection effects. These corrections have been described by Pless.[9]

Opposite each camera is a ground glass screen illuminated by a flash lamp to provide a bright field against which the bubbles appear as dark spots.

The two pictures are reprojected side by side at 3.5 times life size and separate measurements are made in each view. The angles are measured with Bruning drafting machines, and the true angles and ranges in space are then calculated. When the reprojected pictures with the images of the etched grids are compared with the same patterns on the chamber itself, no distortions appear. A discrepancy of 5′ in angle or 0.2% in over-all magnification would be detected.

We thus conclude that all distortions and alignment errors in the optical system are negligible.

The resolution of the optical system is optimized by reducing the f stop of the cameras to the point ($f20$) at which the blurring due to poor focus at the near and far limits of the object is reduced to the same order of magnitude as the diffraction effects of the small camera aperature. Both these effects transform points in the chamber into patterns on the film of dimensions somewhat greater than the resolving power of the film (Linograph Ortho film: 95 lines/mm). The combination of these effects gives an over-all resolving power of about 10 lines/mm in the chamber.

With this resolving power the details of the bubble tracks become clear when the bubbles reach a diameter of 0.15 mm. This bubble size is reached about 3.5 msec after the particle traverses the chamber. The delay between the coincidence counter pulse and the firing of the flash lamps is set accordingly. The scintillation coincidence counters are placed as shown in Fig. 1.

The absence of errors in the optical system allows us, within the limits of our resolution, to test for errors associated directly with the bubble tracks. A careful examination of high-energy particle tracks in all regions of the chamber, including some parallel to the axis and others crossing the chamber at various angles, has revealed no deviations from straight lines to suggest turbulence or other spurious curvatures. A radius of curvature less than 200 cm could be easily detected in a 10-cm track. Low-energy meson tracks, on the other hand, are multiply scattered and show considerable deviations from straight lines. This effect limits the measurement of 20-Mev meson scattering angles to an accuracy of about $\pm 1.5°$.

The energy of a scattering event is determined by the range of the recoil proton. Thus a typical proton recoiling 7.75 ± 0.30 mm or 46.5 ± 1.8 mg/cm^2 from a pion scattered through 112° indicates an incident pion energy of 26.0 ± 1.3 Mev. The accuracy of this measurement depends on the bubble size (about 0.15 mm), the number of bubbles per centimeter (about 35),[8] and the uncertainty in our knowledge of the hydrogen density at the time of the photograph.

The figure for the hydrogen density is obtained from a measurement of the equilibrium vapor pressure of the hydrogen at the temperature of operation (5.90 ± 0.05 atmos indicating a temperature of 28.2°K) and a measurement of the pressure at the time of the photograph (2.0 ± 0.5 atmos). With these figures one can extrapolate the known vapor pressure density data[10] to obtain the value

$$\rho = (0.058\pm0.001) \text{ g cm}^{-3}.$$

The uniformity of the tracks throughout the chamber indicates that the temperature must be uniform to within 0.2°K.

Examples of photographs taken with this apparatus appear in references 3 and 8.

III. MESON BEAM

A suitable beam for this experiment should have an energy low enough so that the analysis of the results will not depend strongly on the assumed P-wave phase shifts (see Sec. V). On the other hand, the energy should be high enough so that a large fraction of the scattering events will produce recoil protons of measurable length. These considerations indicate a desirable energy of 15 to 20 Mev. Other important beam properties are, of course, adequate intensity and an adequate fraction of pi mesons.

To produce a beam of these characteristics the following arrangement was used: The pions, which were produced in a 6-mm thick beryllium target exposed to the 450-Mev proton beam of the cyclotron, were focussed by the fringing field into a nearly parallel beam and then passed through a hole in the shielding wall into the experimental area. There they were deflected 68° by a wedge magnet and brought to a focus about a meter from the edge of the magnet pole.

The general features of the beam were determined by taking a range curve with a telescope of three scintillation counters (see Fig. 2). Adding the copper equivalent (4.2 g cm^{-2}) of the counter telescope to the observed range, we find a range for the incident particles corresponding to a pion energy of 56 Mev. This agrees well with the value (55 Mev) computed from the deflection

[9] Irwin A. Pless, thesis, University of Chicago, 1956 (unpublished); also Phys. Rev. **104**, 205 (1956). See also N. Campbell and I. Pless, Rev. Sci. Instr. (to be published).

[10] Wooley, Scott, and Brickwedde, J. Research Natl. Bur. Standards **41**, 379 (1948); A. Euken, Verhandl. deut. physik. Ges. **18**, 18 (1916); Johnston, Keller, and Friedman, J. Am. Chem. Soc. **76**, 1482 (1954).

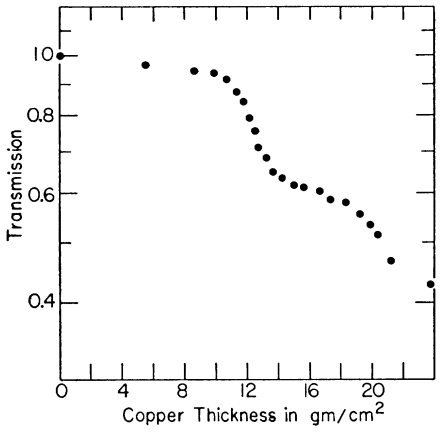

FIG. 2. Range curve for mesons traversing counter telescope. The first drop in transmission occurs at the range predicted for pions using the observed magnetic deflection. The remaining particles are mu mesons and electrons.

by the wedge magnet. The fraction of pions indicated by the range curve is about 38%, the remainder being mu-mesons and electrons of higher energies.

When the bubble chamber was moved into place near the focus of the meson beam the total absorber, including counters, beryllium disks, bubble chamber walls, and 5 cm of hydrogen was adjusted to be 13.7 g copper equivalent, which moderated the pions to about 19 Mev at the center of the hydrogen.

During the experiment the beam intensity was reduced to about half its maximum value in order to give an average of about 2 tracks per picture, since this number was found to allow the optimum rate of scanning.

The best determination of the pion energy distribution was not obtained from the range curve but was computed from the observation of π-μ decay events in the bubble chamber. This technique and the distribution obtained by it are described in the following section.

IV. SCANNING TECHNIQUE AND DATA

Some 75 000 pairs of pictures containing about 4 kilometers of pion track had to be scanned in such a way as to give reliable figures for the total pion track length, the energy distribution of the pion beam, and the energy and angle of each pion scattering event. The scanning rules were chosen in an attempt to maximize the efficiency for detecting events while allowing a reasonably high scanning speed.

We shall first describe the technique, rules, and efficiency of the scanning, and then discuss the analysis of the measurements.

(A) Scanning Procedure

The scanner sits at a table onto which the two views of the chamber are projected side by side. He first decides whether the pair of pictures is free of faults which could impair the reliability of the measurements. He requires that not more than eight tracks be visible entering the chamber. He also disqualifies pictures in which there is an obvious fault in the operation of either camera or light source. Usually such faults occur in a number of successive pictures. In a good roll of film nearly every picture is acceptable.

If the picture is acceptable the scanner then looks for deflections in the tracks. No deflections occurring within 4 mm of the chamber wall are recorded since π-p scattering events this close to the wall could give recoil protons ending in the glass instead of in the hydrogen. The range of such protons could not be measured.

All deflections in the acceptable region of the chamber for which the projected angle in either view is greater than 5° are measured and recorded. As an aid in detecting small angles, mirrors are placed at the sides of the scanning table in such a way that the scanner can easily sight along the tracks.

True angles in space are computed from the measurements of the two projected views.

(B) π-p Scattering Events

A three-pronged event for which the short (proton) prong ends in the chamber and is longer than 0.45 mm is classed as an observable π-p scattering event, provided it satisfies the tests of coplanarity and proper relationship between the pion and proton angles. The minimum track length of 0.45 mm, which corresponds to a recoil proton energy of 2 Mev, is fixed, somewhat arbitrarily, to insure adequate accuracy in determining the energy of the event. This limit on the proton range imposes an energy-dependent lower limit on the range of acceptable pion scattering angles which must be considered in analyzing the results. Table I shows how the minimum angle varies throughout the energy range of the experiment.

Table II lists the 57 observed π-p events. The letter f after an event means that the incident pion satisfied the same limitations on direction and position as the tracks which were used to determine the pion flux. The 28 events of this type may be used in determining the total cross section. All 57 may be used to determine the angular distribution.

An estimate of the efficiency for finding π-p events

TABLE I. Pion scattering angles corresponding to the minimum acceptable recoil proton track length (0.45 mm). Energies and angles are given in the center-of-mass system.

Pion energy Mev	Angle for minimum-length proton track
6	91.2°
9	71.4°
12	60.5°
15	53.2°
18	48.0°
21	44.1°
24	41.0°

TABLE II. List of pion scattering events.

cm energy (Mev)	cm scattering angle	cm energy (Mev)	cm scattering angle
4.9	109° 45′	13.1	69° 59′ *f*[a]
5.9	120° 30′	13.5	139° 52′ *f*
7.2	112° 52′ *f*[a]	13.6	120° 14′
7.5	79° 33′	13.8	77° 18′
8.3	117° 12′	13.8	110° 39′
8.6	89° 26′	14.2	83° 38′
8.6	93° 48′ *f*	14.6	60° 53′ *f*
8.8	83° 01′	14.7	89° 00′
9.0	145° 26′	14.8	105° 22′ *f*
9.8	77° 34′ *f*	14.9	80° 43′ *f*
9.8	111° 43′ *f*	15.2	75° 58′ *f*
10.5	111° 26′	15.7	62° 19′
10.5	148° 11′	15.7	70° 32′ *f*
10.5	162° 16′ *f*	16.4	76° 27′
10.7	110° 57′ *f*	16.4	132° 54′ *f*
11.3	72° 54′ *f*	16.8	128° 02′ *f*
11.4	75° 39′	17.4	56° 52′
11.4	168° 38′	17.4	85° 06′
11.8	76° 55′ *f*	17.8	65° 52′ *f*
12.0	68° 21′ *f*	17.9	89° 47′ *f*
12.0	98° 56′	18.6	56° 07′
12.2	65° 23′	19.1	90° 37′ *f*
12.3	81° 22′	19.3	90° 23′
12.3	82° 12′ *f*	19.3	121° 24′
12.5	131° 41′	22.2	61° 11′ *f*
12.5	147° 54′	22.6	64° 52′ *f*
12.7	59° 05′ *f*	23.7	57° 35′ *f*
12.8	58° 40′	34.2	37° 30′ *f*
12.8	103° 46′ *f*		

[a] The letter *f* following a scattering angle in columns two and four indicates that the event is a "flux event" as defined in Sec. IV.

was made by comparing the number of events seen by two scanners who scanned a common strip of film. The second scanner saw 18 of the 19 events found by the first and no others. On the basis of this test we estimate an average scanner efficiency for π-p events of about 97%. This figure is taken into account in computing the appropriate pion track length [Eq. (2)].

(C) Track Deflections with No Recoil: Pion Flux and Energy Distribution

A deflection with no visible recoil track is recorded as a "kink." Such events may be π-μ decays, low-energy π-p scattering events, electron scattering events, μ-e decays, or μ-p scattering events. Measurement of these kinks provides a basis for determining the pion flux and energy distribution (see below). In order to relate such a flux determination to the π-p events in an unambiguous way, it is necessary to place certain restrictions on the direction of the incident track and on the position at which it enters the chamber.

A total of 1149 kinks were found which satisfied the above criteria and which had true angles greater than 8 degrees. To determine the efficiency of the scanners for finding kinks, film containing 257 kinks was rescanned once. The average efficiency was found to be 89%. No appreciable angular dependence of the efficiency was found. Taking into account the film which was rescanned, the kink efficiency for all the film was 92%±2%. This correction is applied in computing the pion track length [Eq. (2)]. The reproducibility for measuring kink angles was ±1.6° (rms deviation).

Using the information of Sec. III that the mean energy of the pions is about 19 Mev and the fraction of pions about 38% we would expect that the kink distribution would have: (a) a peak near 30° due to π-μ decays, since the pion velocity is such as to favor this laboratory decay angle, (b) a sharp rise in the forward direction due to Coulomb scattering of pions, muons, and electrons, and (c) very few events beyond 50° since such events cannot be due to π-μ decays except at the lower extreme of our energy range and since μ-e decays are expected to contribute less than 1% to the total number of kinks.

The actual distribution which is shown in Table III has exactly these features. Since most of the kinks are π-μ decays and since the angles of these events depend on the pion velocities the kink distribution may be used to infer the pion energy distribution. An analysis of this type was made using an IBM 701 computer, by making a least-squares fit to a linear combination of five distributions corresponding to decays of 10-, 15-, 20-, and 25-Mev pions, respectively, plus a distribution characteristic of the scattering of 20-Mev pions. The last distribution function was chosen to represent all Coulomb scattering of electrons, mesons, and pions. Because of the small overlap of the pion decay functions

TABLE III. Kink distribution. The number of deflections with no visible recoil is listed as a function of angle.

Initial angle (degrees)	Interval (degrees)	No. of kinks[a]
8	2	112
10	2	66
12	2	56
14	2	57
16	2	62
18	2	58
20	2	64
22	2	71
24	2	98
26	2	101
28	2	100
30	2	90
32	2	66
34	2	50
36	2	39
38	2	27
40	2	21
42	2	22
44	2	15
46	2	7
48	2	12
20	2	5
52	2	7
54	2	6
56	2	6
58	2	3
60	10	10
70	10	9
80	10	4
90	30	6
120	30	7
150	30	1

[a] This list includes 109 events which can properly be applied to the kink angular distribution but which should not be included in the flux determination.

TABLE IV. Energy distribution of pions as determined from kink analysis.

Pion energy (Mev)	No. of decays	km of pion track
10	102±18	0.30±0.052
15	320±34	1.15±0.12
20	369±45	1.54±0.18
25	132±39	0.62±0.18

with the last function, the result of the analysis is insensitive to the details of its assumed shape. Only the goodness-of-fit is harmed by a poor estimate of the Coulomb scattering distribution. This point was checked by altering the assumed shape of the scattering distribution and repeating the calculation.

The result of the analysis is shown in Table IV. The flux at each energy has been converted to km of pion track using a pion lifetime of $(2.54\pm0.10)\times10^{-8}$ sec.[11] The distribution given in the table was then smoothed by fitting a Gaussian distribution to it. The track length is then given by

$$L(E)=3.054\times10^{4}\times(1\pm0.086)\times\exp[-0.02(E-18.7)^{2}]\text{ cm Mev}^{-1}, \quad (1)$$

where E is the pion energy in the laboratory system in Mev. The error given in Eq. (1) is the standard deviation of the total track length as computed from Table IV compounded with the error in the pion life time. The effect of errors in this expression on the final result will be discussed in Sec. V.

As a rough check on this method for determining the track length, the total number of tracks passing through the chamber was counted on a portion of the film. This count combined with the chamber length and the information on the fraction of pions in the beam (see Sec. III) indicated a pion track length of $(8.1\pm1.3)\times10^{4}$ cm while the pi-mu decay technique indicated a length of $(8.5\pm1.0)\times10^{4}$ cm for the same portion of film. Track counting was discontinued for the remainder of the scanning since the other technique was faster and more reliable.

The track length in protons cm^{-2} Mev^{-1} is found by multiplying Eq. (1) by $3.375\times10^{22}(1\pm0.033)$, which is the product of Avogadro's number, the hydrogen density, the correction factor for scanning efficiencies, and the factor for the extra kinks mentioned in the footnote to Table III. The error shown is compounded of the errors in the above factors. Our final expression for the track length is

$$n(E)=1.031(1\pm0.092)\times10^{27}\exp[-0.02(E-18.7)^{2}]\text{ atoms cm}^{-2}\text{ Mev}^{-1}. \quad (2)$$

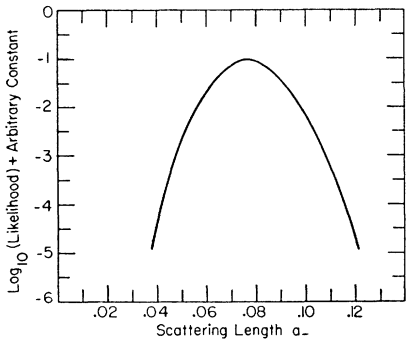

FIG. 3. Logarithm of the likelihood function *vs* scattering length.

V. ANALYSIS OF RESULTS

The final experimental results are presented in the list of π-p events (Table II) corresponding to the pion energy spectrum given by Eq. (2) and to the angular range limited as shown in Table I.

The differential scattering cross section of the process $\pi^{-}+p\rightarrow\pi^{-}+p$ is related, at low energies, to the scattering length a_{-} by the expression[12]

$$d\sigma/d\Omega=\lambda_{C}^{2}\{(a_{-}+e^{2}[\hbar c\eta\beta(1-\chi)]^{-1}+\tfrac{2}{3}\alpha_{33}\chi\eta^{-1})^{2}+(1/9)\alpha_{33}^{2}\eta^{-2}(1-\chi^{2})\}, \quad (3)$$

where λ_C is the pion Compton wavelength, α_{33} is the phase shift for the $P_{\frac{3}{2}}$, isotopic spin $\frac{3}{2}$ state (the other P-wave phase shifts are assumed to be negligibly small in this energy range), χ is the cosine of the c.m. scattering angle of the pion, η is the c.m. momentum (in units of $m_\pi c$), and β is v_π/c in the laboratory system.

For α_{33}, we use the expression

$$\alpha_{33}=0.235\eta^{3}, \quad (4)$$

which comes from higher energy experiments.[13] (The effect of altering this expression is discussed in Sec. VI.) Since these assumptions have also been made by

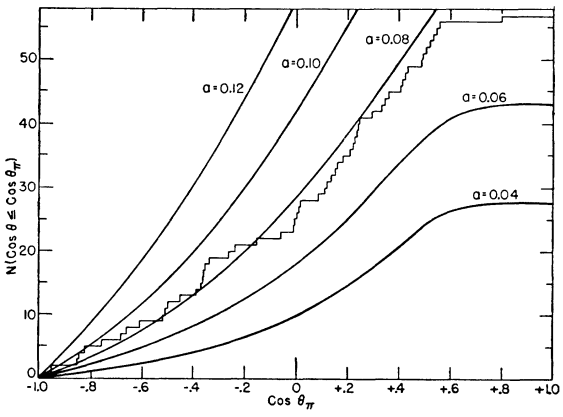

FIG. 4. Integral angular distributions for pion-proton scattering. The smooth curves are calculated for various values of a_{-}, taking into account the energy spectrum and the dependence of the observable angular range upon the energy. At each angle, θ_π, the curves show the total number of events expected for all angles $\theta\leq\theta_\pi$.

[11] Jacobsen, Shulz, and Steinberger, Phys. Rev. **81**, 894 (1951); Durbin, Loar, and Havens, Phys. Rev. **88**, 179 (1952).

[12] L. van Hove, Phys. Rev. **88**, 1358 (1952).

[13] J. Orear, Phys. Rev. **96**, 176 (1954).

Rinehart *et al.*[2] and Orear *et al.*[1] in analyzing their π^- scattering data, a direct comparison of their experiments with ours is possible.

Using a maximum likelihood technique, we have determined the value of a_- which makes the observed distribution of events most probable. The likelihood function is plotted against a_- in Fig. 3. The best value is

$$a_-=0.077\pm0.011. \quad (5)$$

Figure 4 shows how the integral scattering distribution varies with the scattering length. The actual distribution is shown for comparison. It should be pointed out that the *shape* of the actual distribution is given by all 57 events while the absolute value is given only by the 28 events which correspond to the pion flux measurement [see Sec. IV(B)].

Although the error in the scattering length which is shown above includes the effect of the uncertainty in the total track length, it does not include the effect of uncertainty in the energy distribution. To test this, a new distribution was assumed with a mean energy

TABLE V. Results of low-energy π^--p scattering measurements.

	Mean energy of pion beam in lab system (Mev)	$2\alpha_1+\alpha_3$
Orear, Slater, Lord, Eilenberg, and Weaver[a]	26	$(0.15\pm0.09)\eta$[b]
Rinehart, Rogers, and Lederman[c]	15	$(0.25\pm0.05)\eta$
Nagle, Hildebrand, and Plano	18.5	$(0.231\pm0.033)\eta$
Combined result		$(0.234\pm0.027)\eta$

[a] See reference 1.
[b] The published result was $4.7°\pm2.7°$ at 26 Mev. η is the center-of-mass momentum in units of $m_\pi c$. The errors are standard deviations.
[c] See reference 2.

shifted by the maximum amount compatible with the errors in the spectrum analysis (i.e., from 18.7 Mev to 16.6 Mev). The data were then reanalyzed and a new scattering length was found which differed from the best estimate by less than 0.001. Accordingly we may neglect this contribution to the error and adopt (6) as our final result.

A calculation of the dependence of the result on α_{33} shows that $\eta^3 da_-/d\alpha_{33}=-0.1$ under the conditions of our experiment. Thus if α_{33} were decreased from $0.235\eta^3$ to, say, $0.210\eta^3$, then the value of a_- would be increased by $(-0.10)\times(-0.025)=+0.0025$ and $(2\alpha_1+\alpha_3)$ would be increased by 0.0075η. Since this change is less than one fourth as large as the error we assign to our result, we may conclude that our analysis is insensitive to changes of the order of 10% in α_{33}.

One should note that the above value of $\eta^3 da_-/d\alpha_{33}$ applies to this experiment only, since the effect of α_{33} changes rapidly with the energy of the mesons and with the angular range observed.

TABLE VI. Results of low-energy π^+-p scattering measurements.

	Mean energy of pion beam in lab system (Mev)	α_3
Whetstone and Stork[a]	21.5	$(-0.098\pm0.014)\eta$[b]
Evans[c]	20	$(-0.13\pm0.03)\eta$
Combined result[d]		$(-0.107\pm0.013)\eta$

[a] See reference 14.
[b] Published result was $\alpha_3=(-0.048\pm0.007)$, $\alpha_{33}=0.013\pm0.013$, $\alpha_{31}=0.000\pm0.016$ at $\eta=0.49$.
[c] See reference 15.
[d] See discussion in Sec. VI.

VI. DISCUSSION

In Table V we summarize the results of the low-energy π^--p scattering experiments. It will be seen that there is no evidence for a nonlinear momentum dependence of the S-wave phase shifts. Since the assumptions and sources of error in these three experiments are similar, and, we believe, well understood, we feel justified in combining the results to get an estimate of the best value for the phase shift combination $2\alpha_1+\alpha_3$. This combined result appears in the last line of the table.

In order to obtain α_1 and α_3 independently, we must use information from other low-energy experiments involving the S-wave phase shifts. The only such experiments depending on similar assumptions and similar sources of error are the low-energy π^+-p scattering experiments. The results of these experiments are summarized in Table VI.[14,15] Again we have combined the results to give a best estimate for α_3. In this case we are not entirely justified in combining the published results as they stand since they involve somewhat different assumptions concerning the P-wave phase shifts (see footnote to Table VI). A more careful treatment of these results is hardly feasible at this time,

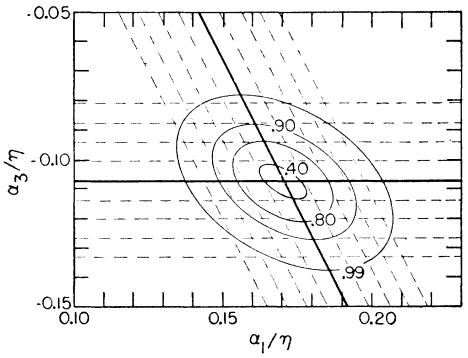

FIG. 5. Results of scattering analysis plotted in the α_1/η, α_3/η plane. The solid horizontal line is the combined result of Table VI (π^+ scattering). The solid diagonal line is the combined result of Table V (π^- scattering). The dotted lines are drawn at intervals of $\frac{1}{2}$ standard deviation. The ovals are contours of equal probability for various combinations of α_1/η and α_3/η. The number on each oval represents the probability that the true result lies within that contour.

[14] S. L. Whetstone and D. H. Stork, Phys. Rev. **102**, 251 (1956).
[15] W. H. Evans, *Proceedings of the CERN Symposium on High Energy Accelerators and Pion Physics, June, 1956* (to be published).

however, since some of the experimental data necessary for a reanalysis have not yet been published and since further experiments of the same type are now in progress.

If we accept the combined result for α_3, then we may obtain a value for α_1 of 0.170η. Since the errors on α_1 and α_3 are related, it is not appropriate to present the phase shifts in the form $\alpha_1 \pm \Delta\alpha_1$, $\alpha_3 \pm \Delta\alpha_3$. Figure 5 shows the results of the π^+-p and π^--p experiments plotted in the α_1/η *vs* α_3/η plane. The intersection of the solid lines gives the best estimate of α_1 and α_3 and the ovals are contours of equal probability for other combinations of α_1 and α_3.

VII. ACKNOWLEDGMENTS

We are indebted to Dr. Irwin Pless for many valuable suggestions and for assistance during the operation of the bubble chamber. We also wish to thank Mr. M. Pyka and Mr. N. Campbell for their help in scanning and analyzing the pictures.

PHYSICAL REVIEW VOLUME 105, NUMBER 2 JANUARY 15, 1957

Pion-Proton Scattering at 220 Mev*

J. ASHKIN, J. P. BLASER,† F. FEINER,‡ AND M. O. STERN§
Carnegie Institute of Technology, Pittsburgh, Pennsylvania
(Received October 8, 1956)

Pion-proton differential scattering cross sections have been measured at 220±7 Mev. Measurements were made at eight angles using scintillation counters and a liquid hydrogen target. Statistical errors range from 5 to 10%. Phase shift analyses have been made of the data in the customary manner. No evidence for d-wave scattering has been found.

INTRODUCTION

IN a recent article[1] we reported on experiments at Carnegie Institute of Technology to measure the angular distribution of negative and positive pions of 150 and 170 Mev scattered in hydrogen. It was found, in agreement with earlier results obtained by Fermi and his co-workers at Chicago, that the data could be analyzed on the assumptions that charge independence was valid in meson-nucleon interactions, and that only s and p waves were strongly scattered. Since it was interesting to see at what point d-wave scattering could no longer be neglected, we decided to do an accurate differential scattering experiment with pions of the highest energy for which the yield in our cyclotron is sufficient. This energy turned out to be 220 Mev and this paper presents the results of the investigation. Measurements at nearly the same energy (217 Mev) have been reported by workers[2,3] at the University of Chicago; the agreement is good. Our corrected cross section values are summarized in Table I. In Table IV we present two sets of phase shifts which give a good fit to our data.

EXPERIMENTAL PROCEDURE

For details on the internally produced negative meson beam, scattering geometry, scintillation counters, hydrogen target, electronics, and experimental procedure, the reader is referred to I.

It had previously been found[4] that for practical purposes the positive pion beam had an upper energy limit of 195 Mev. To extend this limit, an externally produced positive pion beam was used. The arrangement is shown in Fig. 1. A bundle of protons coming out of the cyclotron is focused horizontally by a wedge magnet onto a carbon target 1.5 in. by 3 in. in cross

TABLE I. Experimental cross sections in the center-of-mass system at 220 Mev, in mb sterad^{-1}. Errors shown include statistical and angle-dependent uncertainties, but do not include an over-all uncertainty in the scale of the cross sections amounting to 5% for the negative pion cross sections and 4% for the positive pion cross sections. $\sigma_\gamma(\theta)$ is the differential cross section for detecting either of the two γ rays resulting from decay of the neutral pion produced in charge-exchange scattering. $\sigma_-(\theta)$ and $\sigma_+(\theta)$ refer to the elastic scattering of negative and positive pions respectively.

$\theta_{c.m.}$	$\sigma_+(\theta)$	$\sigma_-(\theta)$	$\sigma_\gamma(\theta)$
37°	18.6±1.1	2.55±0.15	7.55±0.22
52°	15.5±0.9	1.68±0.11	6.51±0.22
70°	9.3±0.8	1.16±0.09	4.70±0.23
90°	5.8±0.7	0.92±0.09	3.71±0.24
110°	6.1±0.8	1.10±0.10	4.11±0.31
128°	9.3±0.9	1.33±0.12	4.95±0.32
143°	14.0±1.1	1.99±0.15	5.23±0.41
162.5°	16.2±1.5	2.60±0.28	6.55±0.57

* Research partially supported by the U. S. Atomic Energy Commission.
† Now at Observatoire Cantonal, Neuchatel, Switzerland.
‡ Now at Knolls Atomic Power Laboratory, Schenectady, New York.
§ Now at General Atomic, San Diego, California.
[1] Ashkin, Blaser, Feiner, and Stern, Phys. Rev. **101**, 1149 (1956), hereafter referred to as I.
[2] M. Glicksman, Phys. Rev. **94**, 1334 (1954).
[3] H. Taft, Phys. Rev. **101**, 1116 (1956).
[4] Ashkin, Blaser, Feiner, Gorman, and Stern, Phys. Rev. **96**, 1104 (1954).